Cell Reports

Report

In Vivo Function of the Chaperonin TRiC in α-Actin Folding during Sarcomere Assembly

Graphical Abstract

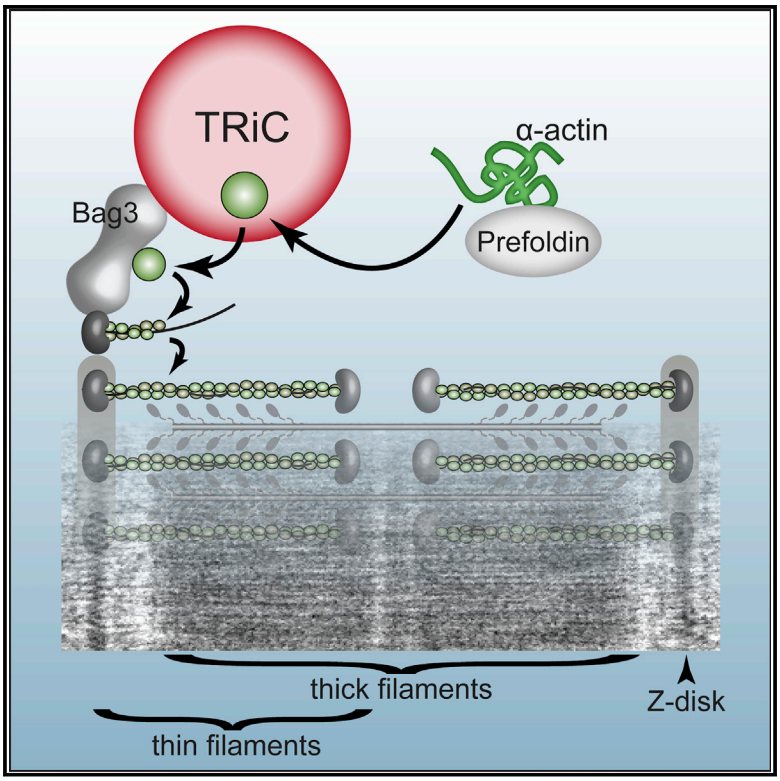

Highlights

- In zebrafish, TRiC loss causes specific defects in sarcomere and neurite formation
- TRiC only enhances the folding of skeletal α-actin at the sarcomeric Z-disk
- ATP binding by Cct5 is required for folding of α-actin, but probably not tubulin
- TRiC function is required for myopathic actin to form rods in nemaline myopathy

Authors

Joachim Berger, Silke Berger, Mei Li, ..., Navid Bavi, Alastair G. Stewart, Peter D. Currie

Correspondence

joachim.berger@monash.edu (J.B.), peter.currie@monash.edu (P.D.C.)

In Brief

TRiC-deficient zebrafish feature specific defects in sarcomere and neurite formation. Berger et al. demonstrate a role for TRiC as a multiprotein scaffold positioned at the sarcomere's Z-disk, where it enhances the processing of skeletal muscle α-actin. Accordingly, TRiC causes aggregation of myopathic α-actin variants in nemaline myopathy.

Berger et al., 2018, Cell Reports *22*, 313–322
January 9, 2018
https://doi.org/10.1016/j.celrep.2017.12.069

CellPress

Cell Reports
Report

In Vivo Function of the Chaperonin TRiC in α-Actin Folding during Sarcomere Assembly

Joachim Berger,[1,2,*] Silke Berger,[1,2] Mei Li,[1,2,3] Arie S. Jacoby,[1,2] Anders Arner,[3] Navid Bavi,[4] Alastair G. Stewart,[5,6] and Peter D. Currie[1,2,7,*]

[1]Australian Regenerative Medicine Institute, Monash University, Clayton, VIC 3800, Australia
[2]Victoria Node, EMBL Australia, Clayton, VIC 3800, Australia
[3]Department of Physiology and Pharmacology, Karolinska Institutet, 17177 Stockholm, Sweden
[4]Department of Physiology, School of Medical Sciences, The University of New South Wales, Sydney, NSW, Australia
[5]Molecular, Structural and Computational Biology Division, Victor Chang Cardiac Research Institute, Darlinghurst, NSW 2010, Australia
[6]Faculty of Medicine, The University of New South Wales, Sydney, NSW 2052, Australia
[7]Lead Contact
*Correspondence: joachim.berger@monash.edu (J.B.), peter.currie@monash.edu (P.D.C.)
https://doi.org/10.1016/j.celrep.2017.12.069

SUMMARY

The TCP-1 ring complex (TRiC) is a multi-subunit group II chaperonin that assists nascent or misfolded proteins to attain their native conformation in an ATP-dependent manner. Functional studies in yeast have suggested that TRiC is an essential and generalized component of the protein-folding machinery of eukaryotic cells. However, TRiC's involvement in specific cellular processes within multicellular organisms is largely unknown because little validation of TRiC function exists in animals. Our *in vivo* analysis reveals a surprisingly specific role of TRiC in the biogenesis of skeletal muscle α-actin during sarcomere assembly in myofibers. TRiC acts at the sarcomere's Z-disk, where it is required for efficient assembly of actin thin filaments. Binding of ATP specifically by the TRiC subunit Cct5 is required for efficient actin folding *in vivo*. Furthermore, mutant α-actin isoforms that result in nemaline myopathy in patients obtain their pathogenic conformation via this function of TRiC.

INTRODUCTION

In eukaryotes, folding of mis- or unfolded proteins is aided by the TCP-1 ring complex (TRiC, also called chaperonin containing TCP-1 [CCT]), a cylindrical structure of two back-to-back rings, each comprised of eight paralogous subunits (CCT1–8) (Gao et al., 1992; Muñoz et al., 2011; Yaffe et al., 1992). Driven by binding and hydrolysis of ATP, TRiC changes its conformation to encapsulate and fold the substrate polypeptides (Joachimiak et al., 2014; Meyer et al., 2003). However, despite the considerable structural data that exist for this complex, the exact mechanism by which TRiC facilitates the folding of its substrates is not fully understood.

In addition to actin and tubulin, the two main substrates of TRiC, it has been estimated that 5%–10% of the proteome of mammalian cells interact with TRiC (Hein et al., 2015; Yam et al., 2008). TRiC loss-of-function mutations in *S. cerevisiae* result in lethality, demonstrating the essential function of TRiC (Stoldt et al., 1996). However, the extent to which TRiC contributes to the folding of its substrates in multicellular, metazoan animals is less explored, and recent *in vivo* studies indicate that TRiC might have specific functions within higher animals, such as autophagy, cell division, and cell migration (Lundin et al., 2008; Pavel et al., 2016). TRiC has also been associated with multiple diseases, including retinal dystrophy (Minegishi et al., 2016), myocardial infarction (Erdmann et al., 2013) and dysfunction (Melkani et al., 2017), sensory neuropathy (Pereira et al., 2017), Parkinson's disease (Sot et al., 2017), and Huntington's disease (Behrends et al., 2006; Tam et al., 2006), suggesting that TRiC components may well be involved in specific cellular processes within distinct tissues.

Zebrafish possess single, highly conserved orthologs for each of the 8 different TRiC subunits that share 85% to 88% sequence identity with humans. Surprisingly, zebrafish *cct* mutants develop into relatively normal larvae with a highly specific skeletal muscle defect. Mutations in *cct* specifically result in impaired folding of skeletal muscle α-actin at Z-disks, causing reduced sarcomere assembly, and characterization of a missense mutation in the ATP binding pocket of Cct5 suggests subunit-specific regulation for the folding of α-actin. In addition, TRiC function induces nemaline rod formation by myopathic actin, implicating TRiC as a potential disease modifier in actin-related myopathies.

RESULTS

A Missense Mutation in the Cct5 Subunit of TRiC Leads to Skeletal Muscle Defects

To study sarcomere assembly in vertebrates, we systematically isolated and characterized mutants that carry defects in sarcomere formation within zebrafish larvae. As part of this approach, we mapped the unresolved mutant *tf212b*, which was previously identified in a genetic screen for mutants with reduced birefringence (Granato et al., 1996). Birefringence is the diffraction of polarized light by the pseudo-crystalline array of the muscle's myofibril and, therefore, a direct measure of myofibril integrity (Berger et al., 2012). Under bright-field microscopy, *tf212b* homozygotes appeared grossly normal (Figure 1A). However,

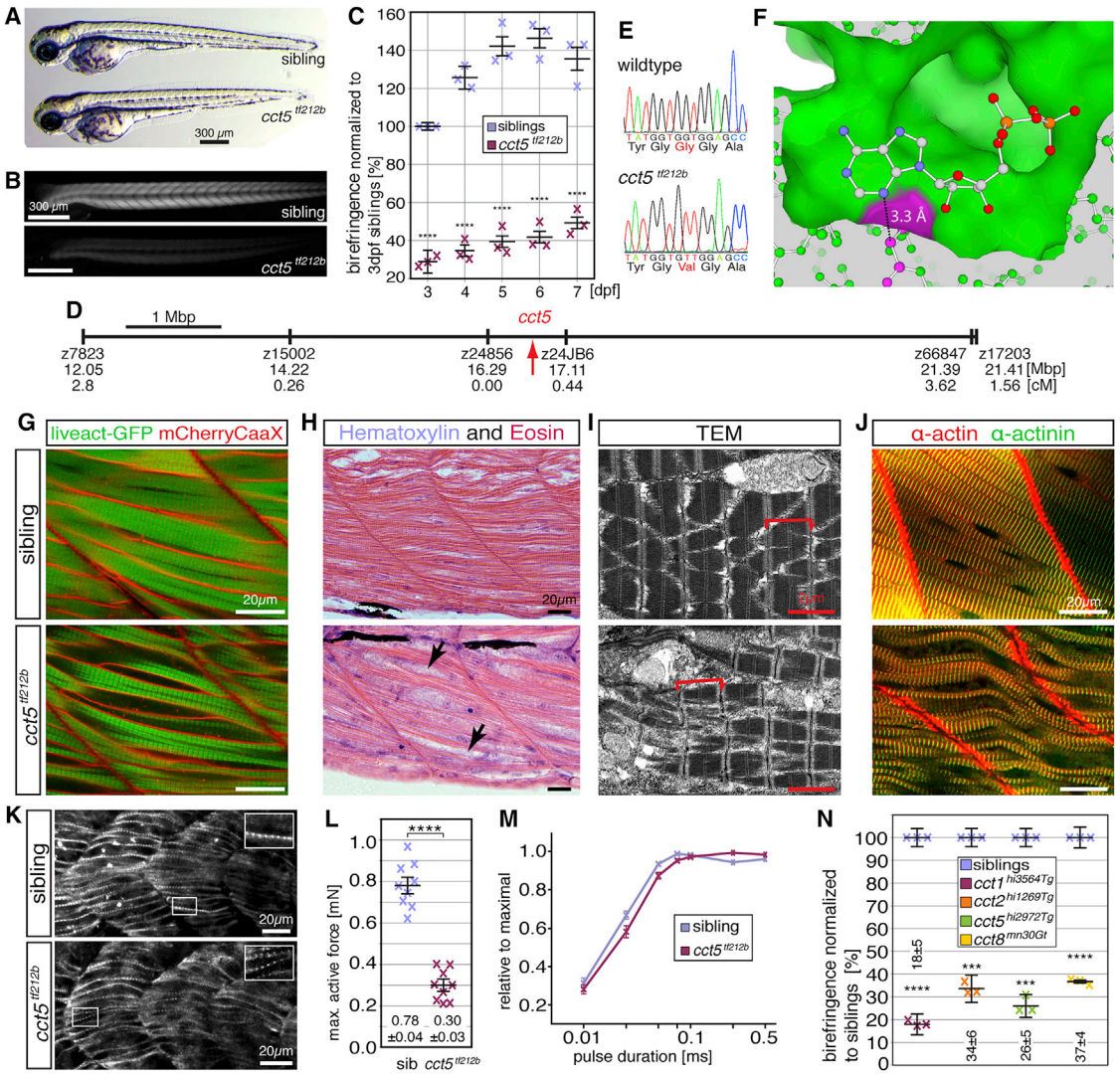

Figure 1. A Missense Mutation in *cct5* Causes Muscle Impairment within *cct5*^{tf212b}

(A) At 3 dpf, *cct5*^{tf212b} mutants appear similar to their siblings under bright-field conditions (n = 6 per genotype).

(B) Representative images of 3-dpf-old *cct5*^{tf212b} mutants under polarized light show a reduction in birefringence (quantified in C).

(C) Quantification of birefringence followed by normalization to 3-dpf-old siblings revealed a highly significant reduction in *cct5*^{tf212b} homozygotes through 7 dpf. Data are mean ± SEM; ****p < 0.0001 homozygotes versus siblings of the same stage by one-way ANOVA with Tukey's *post hoc* test; n = 3.

(D) SSLP-based mapping linked the phenotype-causing mutation to *cct5* on chromosome 24. SSLP positions are shown in centimorgans and million base pairs according to the zebrafish genome assembly. Scale bar, 1 Mbp.

(E) Sequencing identified a missense mutation in exon 9 of *cct5* (G422V).

(F) G422 (pink) forms part of the ATP-binding pocket (surface representation, green) of human CCT5. The glycine carbon is only 3.3 Å away from the adenosine nitrogen (stick representation, blue).

(G) Labeling of the sarcolemma with mCherryCaaX and the myofibril with Lifeact-GFP confirmed a reduced amount of myofibrils within *cct5*^{tf212b} homozygotes (n = 4 per genotype).

(H) H&E-stained sagittal sections of 6-dpf-old larvae confirmed the reduced amount of myofibrils in *cct5*^{tf212b}; arrows mark enlarged regions of the sarcoplasm (n = 8 per genotype).

(I) Representative transmission electron micrographs depicting organized sarcomeres, marked by brackets, in 3-dpf siblings and *cct5*^{tf212b} mutants (n = 3 per genotype).

(J) Immunohistochemistry with antibodies against actin (red) and α-Actinin (green) enabled quantification of the sarcomere width that was not altered in *cct5*^{tf212b} (n = 3 per genotype).

(K) At the 18-somite stage, regularly spaced actinin-positive Z-bodies indicate the presence of pre-myofibrils in siblings and *cct5*^{tf212b} homozygotes (n = 4 per genotype).

(L) Maximal force generation of *cct5*^{tf212b} were significantly impaired compared with siblings. Data are mean ± SEM; ****p < 0.0001 by Student's t test; n = 9.

(legend continued on next page)

polarized light revealed a highly significant reduction in birefringence that persisted to 7 days post-fertilization (dpf), indicating a severe reduction in the amount of myofibrils (Figures 1B and 1C). Mapping of *tf212b* linked the phenotype-causing mutation to the gene encoding the TRiC subunit Cct5 on chromosome 24 (Figure 1D). Subsequent sequencing identified a missense mutation in *cct5* resulting in a glycine-to-valine substitution at position 422, which constitutes part of the conserved ATPase domain (Reissmann et al., 2012; Figures 1E and 1F). The crystal structure of the human ortholog CCT5 (Pereira et al., 2017), which is 87% identical to zebrafish Cct5, shows that the distance between the G422 carbon and adenosine nitrogen of ADP is only 3.3 Å (Figure 1F) and is therefore unlikely to accommodate a valine substitution. Furthermore, molecular dynamics simulations on the wild-type (WT) and G422V mutant protein resulted in structural changes of the ATP binding pocket, a reduction in interaction energy, and ejection of nucleotide on the nanosecond timescale (Figures S1A–S1E). This analysis implies that the G422V mutation results in ATPase-deficient Cct5 protein. The G422V-harboring *cct5* mutant was subsequently named *cct5*^{tf212b}.

Knockdown of *cct5* by two independent morpholinos, both validated for their functionality, resulted in a reduction of birefringence comparable with *cct5*^{tf212b} homozygotes (Figures S2A–S2G). Furthermore, a second mutant allele of *cct5*, *cct5*^{hi2972Tg}, which carries a single retroviral insertion in *cct5* (Amsterdam et al., 2004), failed to complement the birefringence reduction of *cct5*^{tf212b} (Figure S2H). In addition, both *cct5* mutants were significantly ameliorated by injection of full-length *cct5* mRNA, confirming that the phenotype-causing mutation of *cct5*^{tf212b} resides within *cct5* (Figures S2I and S2J).

The Skeletal Muscle Pathology of *cct5*^{tf212b} Mutants Results in Muscle Weakness

The reduced amount of myofibril in *cct5*^{tf212b}, indicated by birefringence, was confirmed in the *Tg(acta1:mCherryCaaX)* and *Tg(acta1:lifeact-GFP)* transgenic background, in which mCherryCaaX highlights the sarcolemma together with t-tubules and Lifeact-GFP directly marks actin thin filaments (Figure 1G; Berger et al., 2014). Accordingly, sagittal sections stained with H&E revealed the enlarged sarcoplasm evident within *cct5*^{tf212b} mutants (Figure 1H). However, transmission electron microscopy (TEM) and immunohistochemistry with antibodies against α-Actinin and actin revealed the typical pattern of striation and preserved sarcomere length within the residual myofibril of *cct5*^{tf212b} mutants (Figures 1I and 1J; data not shown). At the 18-somite stage, immunolabeling of Z-bodies with antibodies against α-Actinin within *cct5*^{tf212b} mutants indicated preserved formation of the pre-myofibril, the first step leading to myofibrillogenesis (Sanger et al., 2010; Figure 1K).

To quantify the physiological effect of reduced myofibril formation in *cct5*^{tf212b}, 5-dpf-old *cct5*^{tf212b} homozygotes and siblings were subjected to mechanical force measurements using a force transducer (Li et al., 2013). Isometric force analysis was performed with entire larvae at various larva lengths to identify the optimal muscle length for maximal active force quantification. After single-twitch stimulation, the generation of maximal active force was significantly reduced in the *cct5*^{tf212b} mutant group compared with siblings (Figure 1L). To assess whether the reduced muscle force was based on defective motor neurons, contractions were analyzed using single-twitch stimulations with different pulse duration because short-duration pulses are motor neuron-dependent (Abramsson et al., 2013). The obtained results revealed a superimposable relationship between the two groups, indicating unaltered excitation responses and fully functional motor neurons within *cct5*^{tf212b} mutant larvae (Figure 1M).

In addition to the trunk muscle, the head musculature of *cct5*^{tf212b} mutants was also affected, as indicated by the highly significant reduction in the length of the hyohyoideus muscle marked by the transgenic line *Tg(−503unc:GFP)* (Berger and Currie, 2013; Figure S3A). In accordance with the reduced head musculature, Alcian blue staining revealed cartilage abnormalities in *cct5*^{tf212b}, preventing mutants from closing their jaw, suggesting that death of *cct5*^{tf212b} mutants at 11 dpf was caused by starvation (Figures S3B and S3C).

Collectively, these analyses reveal that *cct5*^{tf212} mutants possess a global skeletal muscle pathology, characterized by a severe reduction in the amount of myofibrils formed within individual muscle fibers. The residual sarcomeric units that do form within mutant fibers appear normal in spacing and length, but the overall reduction in myofibrils results in a severe reduction in skeletal muscle-dependent force generation.

Mutations in Other TRiC Subunits Also Cause Impaired Myofibril Assembly

To assess whether the myofibril phenotype of the *cct5* mutants is subunit-specific, a number of distinct TRiC subunit mutants were analyzed. In previous large-scale gene trap screens, mutations in subunits Cct1 (*cct1*^{hi3564Tg}), Cct2 (*cct2*^{hi1269Tg}), Cct5 (*cct5*^{hi2972Tg}), and Cct8 (*cct8*^{mn30Gt}) have been identified, although detailed phenotypic information is missing on all these mutants (Amsterdam et al., 2004; Petzold et al., 2009). Birefringence analysis of all four mutants revealed a highly significant birefringence reduction in each mutant (Figure 1N). Similar to *cct5*^{tf212b}, muscle phenotypes of all analyzed *cct* mutants were evident on H&E-stained cross-sections, which revealed increased amounts of endomysial connective tissue (Figures S4A–S4E). Accordingly, TEM analysis of all gene trap mutants revealed a reduced amount of myofibrils with otherwise preserved sarcomere organization (Figures S5A–S5D). These results indicate that mutations in three other TRiC subunits result in a muscle phenotype highly similar to that evident in *cct5*^{tf212b}.

Because the gene trap alleles and the *cct5*^{tf212b} missense mutation likely result in partial loss-of-function phenotypes, we sought to examine full null mutations. The *cct3*^{sa1761} mutant

(M) Pulse duration and active force relationships are similar in both groups, suggesting unchanged motor neuron excitation. Data are mean ± SEM; n = 10.
(N) The insertion mutants *cct1*^{hi3564Tg}, *cct2*^{hi1269Tg}, *cct5*^{hi2972Tg}, and *cct8*^{mn30Gt} all feature a highly significant reduction in birefringence. Data are mean ± SEM; ***p < 0.001 and ****p < 0.0001 by Student's t test; n = 3.
See also Figures S1–S5.

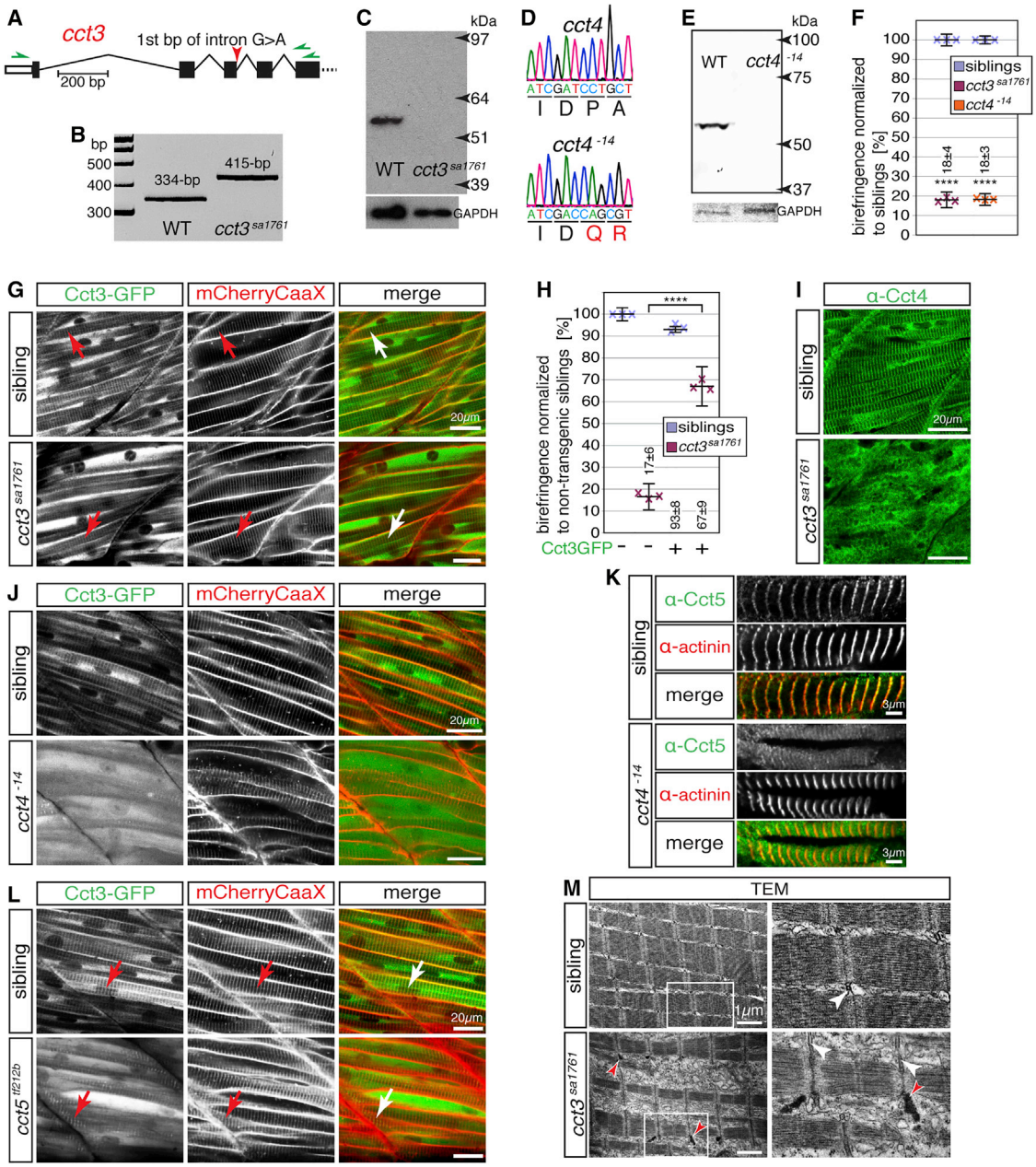

Figure 2. Loss of TRiC Subunits Causes Lack of Functional TRiC at Sarcomeric Z-disks

(A) *cct3*^{sa1761} harbors an essential splice site mutation in *cct3* (red arrow).

(B) RT-PCR using oligonucleotides targeting regions marked by green arrows in (A) generated a 334-bp amplicon with WT embryos and a single 415-bp amplicon with *cct3*^{sa1761} homozygotes. Amplicons were identified by sequencing.

(C) Western blot analysis using antibodies against human CCT3 revealed epitope loss in *cct3*^{sa1761} homozygotes (GAPDH served as a loading control).

(D) CRISPR/Cas9-mediated deletion of 14 bp from exon 5 of *cct4* causes a frameshift evoking premature stop codons in *cct4*$^{-14}$.

(E) Western blot analysis using antibodies against CCT4 revealed epitope loss in *cct4*$^{-14}$ homozygotes (GAPDH served as a loading control).

(F) At 3 dpf, the birefringence was significantly reduced in *cct3*^{sa1761} and *cct4*$^{-14}$ mutants compared with siblings. Data are mean ± SEM; ****p < 0.0001 by Student's t test; n = 3.

(G) GFP fluorescence of *Tg(cry:mCherry,-600unc:cct3GFP)* localized to sarcomeric Z-disks as identified by co-localization with mCherryCaaX-positive t-tubules introduced by *Tg(acta1:mCherryCaaX)* in siblings and *cct3*^{sa1761} homozygotes (arrows) (n = 5 per genotype).

(H) Expression of the Cct3-GFP fusion protein ameliorated the birefringence of *cct3*^{sa1761} homozygotes with high significance. Data are mean ± SEM; ****p < 0.0001 by one-way ANOVA with Tukey's *post hoc* test; n = 3.

(I) The striated pattern obtained with antibodies against Cct4 in siblings was severely compromised in *cct3*^{sa1761} (n = 5 per genotype).

(legend continued on next page)

allele, generated by the Sanger Mutagenesis Project, harbors an essential splice site mutation (G > A) in the first base pair after exon 3 of *cct3* (Figure 2A). Aberrant splicing of *cct3* transcript in *cct3*^{sa1761} was demonstrated by RT-PCR, and subsequent sequencing revealed inclusion of the 81-bp intron into the *cct3*^{sa1761} transcript, resulting in additional in-frame premature stop codons (Figure 2B). Loss of the Cct3 epitope in *cct3*^{sa1761} homozygotes was confirmed by western blot analysis using antibodies against human CCT3 (Figure 2C). In addition, a *cct4* mutant was generated by CRISPR/Cas9 technology that harbors a 14-bp deletion in exon 5 that induces a frameshift after the codon for D190 (Figure 2D). The loss of the Cct4 epitope was confirmed by western blot (Figure 2E). In contrast to CCT-deficient yeasts that die of cytoskeletal defects (Stoldt et al., 1996), *cct3*^{sa1761} and *cct4*$^{-14}$ null mutants developed into relatively normal larvae that exhibited skeletal muscle defects grossly similar to the other *cct* mutants described above. H&E-stained cross-sections revealed a similar increase in endomysial connective tissue within *cct3*^{sa1761} and *cct4*$^{-14}$ 3-dpf-old homozygotes (Figures S4F and S4G). However, at 3 dpf, the birefringence of *cct3*^{sa1761} and *cct4*$^{-14}$ homozygotes was further reduced to levels below that evident within the other analyzed *cct* mutants (Figure 2F), which strengthens the notion that TRiC is partially functional in these other mutants. The reduced level of myofibril formation within *cct3*^{sa1761} and *cct4*$^{-14}$ homozygous mutants was confirmed in the transgenic background of *Tg(acta1:mCherryCaaX)* and *Tg(acta1:lifeact-GFP)*, and regularly spaced Z-bodies were detected in *cct4*$^{-14}$ homozygotes by antibodies against α-Actinin, indicating pre-myofibril formation (Figures S4H–S4J).

TRiC Assembles at Sarcomere Z-disks, with Loss of Individual Subunits Abolishing Z-disk Localization

To identify the cellular localization of TRiC within skeletal muscle cells, the transgenic line *Tg(cry:mCherry,-600unc:cct3GFP)* was generated, in which the *αA-crystallin* promoter reports transgenesis by driving mCherry expression in the lens, and GFP-tagged Cct3 expression is directed to the musculature by the *unc-45b* promoter (Berger and Currie, 2013). To prevent GFP from interfering with TRiC formation and function, GFP was integrated in the apical domain of the Cct3 subunit in a manner similar to studies performed in yeast, in which this tag location preserved CCT function (Pappenberger et al., 2006). In both siblings and rescued *cct3*^{sa1761} homozygotes, Cct3-GFP protein was localized to Z-disks, which were indicated by mCherryCaaX-positive t-tubules marked in the *Tg(acta1:mCherryCaaX)* line (Figure 2G). Expression of GFP-tagged Cct3 in the musculature significantly ameliorated the muscle integrity deficits of transgenic *cct3*^{sa1761} homozygotes, as evaluated by birefringence analysis, indicating that the fusion protein was functional and integrated normally into TRiC (Figure 2H). The TRiC localization was also confirmed by immunohistochemistry with antibodies against CCT4 performed in siblings (Figure 2I). However, Cct4 localization was severely compromised in *cct3*^{sa1761} mutants, indicating that TRiC was not assembled at the Z-disk in Cct3 deficiency. To validate the subunit specificity of this finding, *cct4*$^{-14}$ was crossed to *Tg(cry:mCherry,-600unc:cct3GFP)*. Localization of Cct3-GFP to Z-disks was not found in *cct4*$^{-14}$ homozygotes, and the fluorescence signal was severely reduced compared with the robust signal detected in siblings, suggesting that TRiC was not assembled at the sarcomere after deletion of only one of the eight TRiC subunits (Figure 2J). Accordingly, antibodies against Cct5 and α-Actinin showed that Cct5 was confined to actinin-positive Z-disks in the skeletal muscle of siblings but not *cct4*$^{-14}$ homozygotes (Figure 2K). However, expression of transgenic Cct3-GFP in the partial loss-of-function mutant *cct5*^{tf212} showed that GFP-tagged TRiC in siblings as well as homozygous *cct5*^{tf212b} was localized to the sarcomere's Z-disk, indicating that TRiC assembles in *cct5*^{tf212b} (Figure 2L).

Next, TEM was performed to examine sarcomere structure within *cct* null mutants. Similar to the myofibril organization in other TRiC mutants, residual sarcomeres in *cct3*^{sa1761} and *cct4*$^{-14}$ were organized (Figure 2M; Figure S5E). However, in contrast to *cct5*^{tf212} homozygotes, abundant electron-dense aggregates were detected, extending outside of sarcomeres specifically at Z-disks, where previously GFP-tagging and immunohistochemistry analyses indicated that TRiC was localized. Collectively, these analyses suggest that loss of individual subunits abolishes TRiC assembly at the sarcomere's Z-disk, which, in turn, causes protein aggregation and arrest of sarcomere assembly.

TRiC Function Is Required for Efficient Folding of Skeletal Muscle α-Actin

To analyze whether the documented muscle phenotypes could be related to a reduction of functional α-actin, morpholino knockdown of the two orthologs of human ACTA1 was undertaken to reduce, but not eliminate, the levels of Acta1 in zebrafish. Administration of the acta1ATG morpholino, which simultaneously targets translation starts of both *acta1b* and *acta1a*, induced a highly significant reduction of birefringence in WT larvae (Figure 3A). The myofibril reduction induced by acta1ATG administration was also apparent in the transgenic background of *Tg(acta1:mCherryCaaX)* and *Tg(acta1:lifeact-GFP)* (Figure 3B). Importantly, residual myofibril organization remained intact after acta1ATG administration (Figure 3C). Therefore, based on the analyzed myofibril reduction and organization, simultaneous

(J) Compared with siblings, localization of Cct3-GFP to Z-disks is severely compromised in *cct4*$^{-14}$ homozygotes transgenic for *Tg(cry:mCherry,-600unc:cct3GFP)* and *Tg(acta1:mCherryCaaX)* (n = 4 per genotype).

(K) Immunohistochemistry detected the localization of Cct5 at actinin-positive Z-disks in siblings but not in *cct4*$^{-14}$ homozygotes (n = 3 per genotype).

(L) In *cct5*^{tf212b} homozygotes and siblings that harbor *Tg(cry:mCherry,-600unc:cct3GFP)* and *Tg(acta1:mCherryCaaX)*, GFP-tagged Cct3 localized to Z-disks (arrows) (n = 3 per genotype).

(M) Representative TEM micrographs of *cct3*^{sa1761} present a reduced amount of myofibrils (n = 3 per genotype). Importantly, although the sarcomeres appear organized, electron-dense rods were detected at Z-disks in *cct3*^{sa1761} (red arrowheads). White arrowheads point to t-tubules at Z-disks. Boxed areas are shown at higher magnification.

See also Figures S4, S5, and S7.

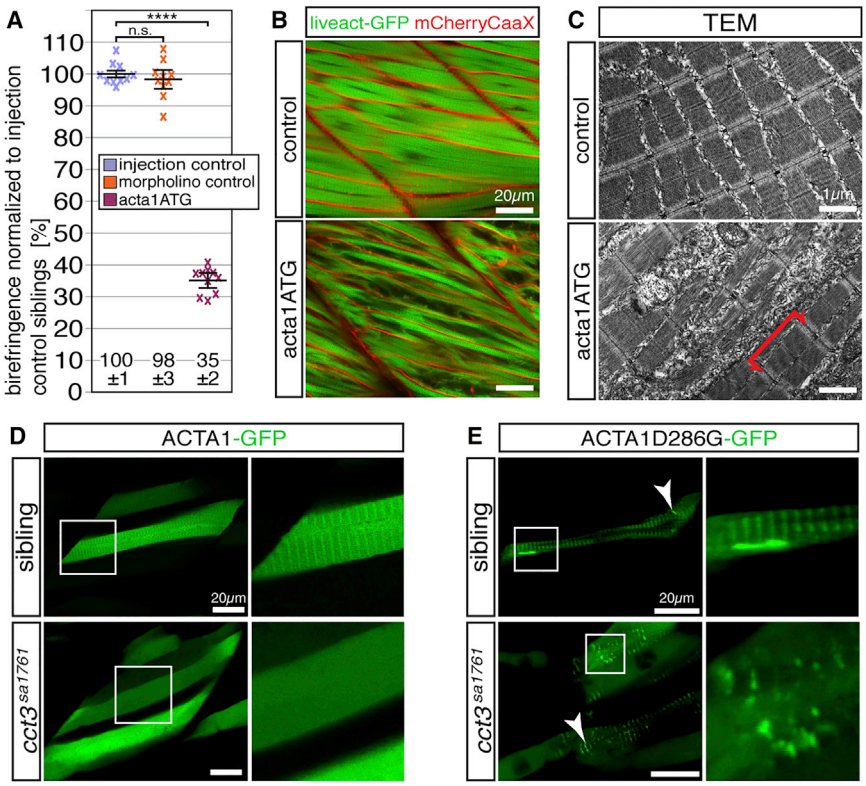

Figure 3. Actin Folding Is Impaired in *cct3*^{sa1761}

(A) Injection of 3-dpf-old WT larvae with 100 μM acta1ATG morpholino targeting *acta1a* and *acta1b* significantly reduced their birefringence in comparison with larvae injected with injection solution (injection control) or 100 μM standard control morpholino (morpholino control). Data are mean ± SEM; ****$p < 0.0001$ by Student's t test; n = 10.

(B) The reduced amount of myofibrils after *acta1a* and *acta1b* knockdown was also documented in the transgenic background of *Tg(acta1:mCherryCaaX)* and *Tg(acta1:lifeact-GFP)* (n = 4 per genotype).

(C) TEM revealed that knockdown of *acta1a* and *acta1b* reduced the amount of myofibrils but did not affect sarcomere organization (n = 3 per genotype).

(D) After incorporation of ACTA1-GFP, the myofibrils of siblings presented a striated fluorescence pattern, whereas the fluorescence of the *cct3*^{sa1761} myofibrils appeared uniform (4 larvae per genotype, each with 5 myofibers analyzed).

(E) Mutant ACTA1^{D286G}-GFP formed rod-shaped structures (arrowhead) in siblings, whereas, in *cct3*^{sa1761} homozygotes, exclusively amorphic aggregates of various sizes (arrowhead) were observed (4 larvae per genotype, each with 5 myofibers analyzed).

See also Figure S6 and Table S1.

knockdown of *acta1a* and *acta1b* resulted in a muscle phenotype similar to that evident in *cct* mutants.

Folding of skeletal muscle myosin has been suggested to be accelerated by TRiC (Srikakulam and Winkelmann, 1999). Accordingly, along with the main substrates actin and tubulin, skeletal muscle myosin was co-immunoprecipitated from 5-dpf-old WT larvae with antibodies against human CCT5 (Table S1). However, administration of the small molecule EMD57033, which refolds myosin (Radke et al., 2014) and significantly ameliorates the birefringence reduction resulting from unfolded myosin in *unc45b* morphants (Figures S6A and S6B; Etard et al., 2015), did not show a significant effect on the birefringence of *cct3*^{sa1761} homozygotes (Figure S6C). These results collectively indicate that deficiencies in myosin folding might not be the main effector of the phenotype of *cct* mutants.

To test whether TRiC loss of function leads to defects specifically in folding of α-actin, GFP-tagged human α-actin (*ACTA1-GFP*), which has been shown to incorporate into sarcomeres (Sztal et al., 2015), was transiently expressed under control of the muscle-specific *unc-45b* promoter. Fluorescence of ACTA1-GFP in siblings resulted in the expected striation pattern, indicating integration of ACTA1-GFP into the myofibril (Figure 3D). In contrast, *cct3*^{sa1761} myofibers presented with a uniform fluorescence, indicating that the majority of ACTA1-GFP was not integrated into the residual myofibril, which suggests that ACTA1-GFP integration into sarcomeres is enhanced by Cct3 activity. Furthermore, GFP-positive aggregates were not detected, neither in siblings nor in *cct3*^{sa1761} homozygotes, indicating that ACTA1-GFP does not aggregate, even at high levels elicited by transgenic overexpression.

TRiC Function Is Required for Nemaline Rod Formation

Nemaline myopathy is a human muscle disorder that is diagnosed by the presence of nemaline rods, rod-shaped electron-dense aggregates that form inside myofibers (North et al., 2014). D286G substitution in ACTA1 has been suggested to cause nemaline rod formation in patients suffering from nemaline myopathy (Ravenscroft et al., 2011). In both mouse and zebrafish, expression of ACTA1^{D286G}-GFP within muscle fibers results in incorporation of the transgenic fusion protein into the myofibril and formation of nemaline rods (Ravenscroft et al., 2011; Sztal et al., 2015). Accordingly, expression of ACTA1^{D286G}-GFP within siblings caused formation of long, rod-shaped nemaline rods and a striated GFP fluorescence pattern resulting from the incorporation of ACTA1^{D286G}-GFP into sarcomeres (Figure 3E). In *cct3*^{sa1761}, however, along with a faint striated GFP pattern, amorphic GFP-positive aggregates were found within ACTA1^{D286G}-GFP-expressing myofibers, and GFP fluorescent nemaline rods were not detected, which confirmed the defective α-actin folding in *cct3*^{sa1761} (Figure 3E). This result revealed that TRiC function is required for nemaline rod formation resulting from the expression of disease-causing skeletal muscle α-actin variants.

ATP Binding by Cct5 Is Specific for Skeletal Muscle α-Actin but Not Tubulin Processing

The other proposed main substrates suggested for TRiC besides actin are α- and β-tubulin (Yaffe et al., 1992), which are the main

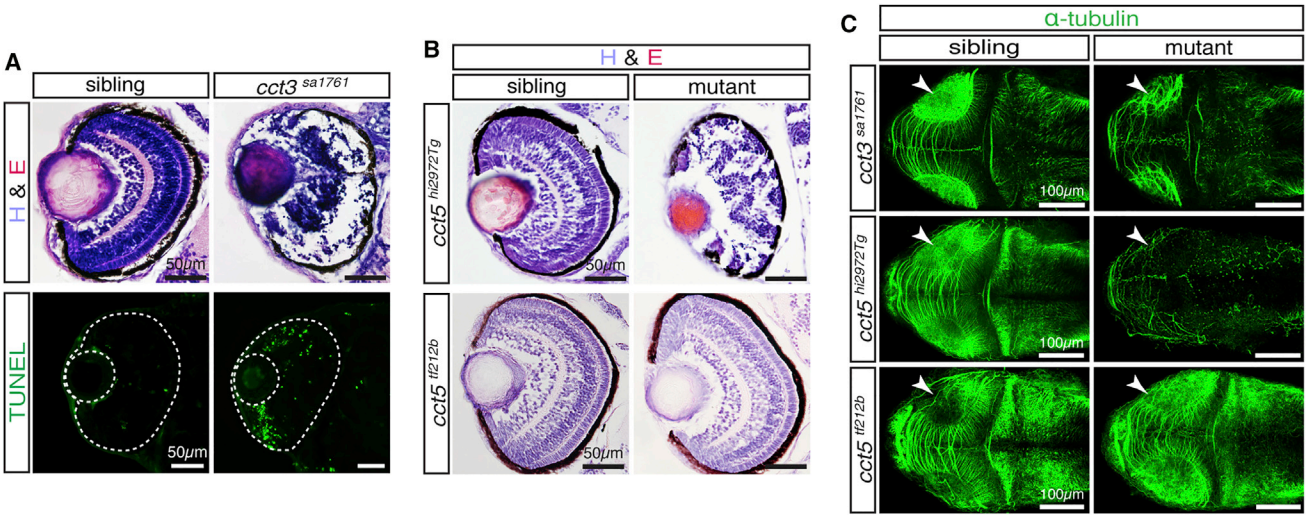

Figure 4. All *cct* Mutants Show Retina Degeneration, Except for *cct5*^{tf212b}

(A) H&E-stained sections of 3-dpf-old *cct3*^{sa1761} mutants showed severe retina degeneration (n = 11 per genotype) accompanied by abundant apoptosis detected by TUNEL assay (n = 6 per genotype).

(B) At 3 dpf, retina degeneration was also apparent on H&E-stained sections of the insertion mutant *cct5*^{hi2972Tg} but not of the missense mutant *cct5*^{tf212b} (n = 11 per genotype).

(C) Pursuant to the retina degeneration, immunohistochemistry with antibodies against acetylated α-tubulin detected neurite defects in the tectum (arrowheads) of *cct3*^{sa1761} and *cct5*^{hi2972Tg} but not *cct5*^{tf212b} homozygotes (n = 4 per genotype).

See also Figure S6.

components of microtubules that are essential for cellular functions, including growth and maintenance of neuronal neurites. The zebrafish *cct3*^{ntn} mutant has been reported previously to have impaired differentiation of retinal ganglion and tectal neurons (Matsuda and Mishina, 2004), and missense mutations in human *CCT2* have been associated with retinal dystrophy and macular degeneration (Minegishi et al., 2016). Accordingly, H&E-stained sections revealed retinal degeneration in *cct3*^{sa1761} accompanied by abundant apoptotic cells, as identified by terminal deoxynucleotidyl transferase dUTP nick end labeling (TUNEL) (Figure 4A). Interestingly, all other analyzed TRiC mutants are characterized by a similar retinal defect, except for *cct5*^{tf212b}, in which the retina appears to develop normally (Figure 4B; Figures S6D–S6G).

Because neuron viability depends on neurites to innervate target tissues (Dubey et al., 2015), and retinal axons connect to the tectum, immunostaining was performed with antibodies against acetylated α-tubulin. This analysis detected a severe reduction of neuronal neurites within the tectum of *cct3*^{sa1761} homozygotes, which would be anticipated from impaired tubulin processing (Kapitein and Hoogenraad, 2015; Figure 4C). However, in contrast to the insertion mutant *cct5*^{hi2972Tb}, similar defects were not observed in the missense mutant *cct5*^{tf212b}, neither on whole mounts stained with acetylated α-tubulin antibodies nor in neuronal transgenic marker lines (Figure 4C; Figures S7A–S7D). Therefore, *cct5*^{tf212b}, which carries a missense mutation in the ATP-binding pocket, is the only analyzed mutant with a muscle-specific phenotype. This result suggests that ATP binding by the Cct5 subunit is specifically required for skeletal muscle α-actin and not tubulin folding by TRiC, providing an indication of how distinct protein folding activities of TRiC may be regulated.

DISCUSSION

In vivo analysis of *cct3* or *cct4* loss of function in zebrafish revealed that loss of one Cct subunit likely prevents assembly of TRiC, a result predicted by the crystal structure of yeast TRiC but lacking *in vivo* validation until our observations. Despite the absence of assembled TRiC, *cct3*^{sa1761} and *cct4*$^{-14}$ homozygotes develop into 5-day-old larvae, which is surprising given the proposed absolute requirement of TRiC for the folding of many substrates (Lopez et al., 2015), including β- and γ-actins, that build the general cytoskeletal architecture of the cell. Our studies of GFP-tagged ACTA1 show impaired folding of skeletal muscle α-actin in *cct3*^{sa1761}, confirming actin as a substrate for TRiC. Importantly, however, pre-myofibril formation is not abolished in *cct4*$^{-14}$, and residual organized sarcomeres are still formed in *cct3*^{sa1761} and *cct4*$^{-14}$ that completely lack Cct3 or Cct4 protein. Assuming that TRiC function is largely abolished by the removal of critical Cct subunits, these results demonstrate that skeletal α-actin can fold into its native conformation and assemble into thin filaments without TRiC function *in vivo*. Similarly, tubulin-based microtubules were detected in residual neuronal axons of the tectum, indicating that α- and β-tubulin can also fold independent of functional TRiC.

Analysis of GFP-tagged Cct3 and immunohistochemistry demonstrates that TRiC localizes to sarcomeres' Z-disks. Accordingly, aggregates are formed only in the loss-of-function mutants *cct3*^{sa1761} and *cct4*$^{-14}$, exclusively next to the Z-disks outside of sarcomeres. Therefore, loss of functional TRiC at the Z-disk might lead to an impaired sarcomere assembly complex that eventually collapses to form the aggregates evident within both *cct* null mutants. It is therefore intriguing to speculate

that TRiC not only plays a role in enhancing the folding of α-actin but might also act as a scaffold for other proteins to confine actin processing to the Z-disk. During translation, nascent α-actin is bound by the co-chaperone prefoldin and subsequently transported to TRiC for folding (Vainberg et al., 1998). Interestingly, the co-chaperone Bag3 has recently been reported to also bind TRiC (Fontanella et al., 2010). Bag3 localizes to the Z-disk, where it binds to the actin-capping protein CapZ, which stabilizes thin filaments together with nebulin (Hishiya et al., 2010; Pappas et al., 2008). Combined with our analysis, these results collectively suggest a mechanism of actin processing in which prefoldin delivers nascent actin to TRiC, which ensures effective folding of α-actin and subsequently passes native α-actin on to its binding partner Bag3. Bag3 binds to CapZ, which, together with nebulin, stabilizes assembling thin filaments. When assembled, thin filaments are capped by tropomodulin-4 and integrated into sarcomeres (Berger et al., 2014), thereby extending the myofibril.

The important role TRiC plays in the processing of skeletal α-actin is also reflected by results showing that nemaline rod formation by ACTA1^{D286G}-GFP was only detected in siblings but not in Cct3-deficient mutants that feature loss of functional TRiC at the Z-disk. This important finding suggests that TRiC may act as a central control point in the pathogenesis of α-actin-associated nemaline myopathies. Considering that the molecular bases of many types of nemaline myopathy remain unknown (North et al., 2014), these results indicate TRiC as a potential modifier and therapeutic target for α-actin-associated nemaline myopathies.

Direct binding of actin to Cct5 has been suggested for the open conformation of TRiC (Llorca et al., 1999), which is in contrast to a more recent study that proposes functional partitioning of TRiC, in which substrates are bound only by the subunits CCT6, CCT8, and CCT3, which locate opposite to the ATP binding subunits CCT4, CCT2, and CCT5 (Joachimiak et al., 2014). The significant role of ATP binding by Cct5 for substrate folding was confirmed by the phenotype of the zebrafish mutant *cct5*^{tf212b}. Interestingly, however, *cct5*^{tf212b} mutants were uniquely characterized by a muscle-specific phenotype and not the degeneration of the retina or neuronal axons evident in other *cct* alleles, suggesting that Cct5 possesses substrate-specific regulatory properties, with folding of α-actin but not tubulin being affected in *cct5*^{tf212b}. In light of a recent study revealing that CCT5 does not directly bind to actin (Joachimiak et al., 2014), one could speculate that the defects in skeletal muscle actin folding in *cct5*^{tf212b} are caused by impaired binding of ATP by Cct5 resulting in an impaired TRiC conformation change rather than by direct binding of actin to Cct5. Interestingly, a mutation in human CCT5 has been reported to be associated with sensory neuropathy (Bouhouche et al., 2006). This reported H147R mutation of CCT5 affects the flexibility of the equatorial domain of CCT5 and leaves ATP hydrolysis by CCT5 unaffected (Pereira et al., 2017; Sergeeva et al., 2013). Although not directly examined, it has been speculated that the sensory neuropathy evident in patients may well result from altered tubulin and microtubule processing (Pereira et al., 2017; Sergeeva et al., 2013). By contrast, the G422V substitution in zebrafish Cct5 we describe in this study likely disrupts ATP binding and affects actin but not tubulin folding. Collectively, these studies suggest a model whereby distinct conformational changes of the CCT5 subunit may regulate the substrate specificity of TRiC. More research is clearly needed, however, to unravel the exact molecular function of CCT5 in regulating the folding of specific substrates by TRiC.

In conclusion, genetic dissection of TRiC function in zebrafish identified a highly unexpected role for this complex in coordinating sarcomere assembly during vertebrate skeletal muscle formation and revealed TRiC as a potential modifier of nemaline myopathy. Our observations suggest a model in which TRiC acts as a multiprotein scaffold positioned at the Z-disk of the forming sarcomere, where it enhances the folding and processing of skeletal muscle α-actin required for efficient thin filament and sarcomere assembly.

EXPERIMENTAL PROCEDURES

Quantification of Birefringence

The Abrio LS2.2 microscope unit was used to automatically image larvae under unbiased polarized light conditions as reported previously (Berger et al., 2012). Images of larvae were analyzed using the software ImageJ, which enabled selection of the first 20 somites of imaged larvae and measurement of the mean of all gray values of the pixels within this selected region. To facilitate comparison of the birefringence from different mutants, gray values were normalized to control siblings, which were set to 100%. To normalize values of siblings, measured gray values (A_1 to A_n) of each larva were multiplied by 100 and divided by the average of all measured gray values of siblings using $A_i \times 100/(\sum_{i=1}^{n} A_i/n)$. To normalize values of mutants, measured gray values (B_1 to B_n) of each larva were multiplied by 100 and divided by the average of the measured gray values of the siblings using $B_i \times 100/(\sum_{i=1}^{n} A_i/n)$. For morpholino and rescue analyses, 10 or 20 larvae were analyzed per genotype (n = 10 and n = 20, respectively). For mutant analyses, normalized values of 6 larvae from the same clutch were averaged, and three independent clutches were analyzed (n = 3).

Statistical Analysis

All data are presented as mean ± SEM. SEM was calculated utilizing error propagation. Statistical significance between two groups was determined by Student's t test, and significance between multiple groups was calculated by one-way ANOVA with *post hoc* Tukey's test. Statistical calculations were performed with the software Prism (GraphPad).

Force Measurement

The 5-dpf larval preparations were mounted with aluminum clips between a fixed hook and a force transducer on a micrometer screw for length adjustment. The preparations were held in 3-(N-morpholino)propanesulfonic acid (MOPS)-buffered physiological solution at 22°C and stimulated via two platinum electrodes. The maximal active force was determined using single-twitch stimulation. Muscles were also stimulated at optimal length where the maximal force was achieved, using different pulse durations (0.01 to 0.5 ms) to examine the excitability of the neuromuscular activation pathway. Although entire larvae were analyzed, the muscle cross-sectional areas of 5-dpf-old larvae were measured to exclude that the difference in active force generation stems from smaller muscles. Importantly, although *cct5*^{tf212b} mutants showed a myofibril reduction, cross-sectional areas of *cct5*^{tf212b} homozygotes and their siblings were similar (0.0326 ± 0.0004 mm^2 and 0.0330 ± 0.0008 mm^2, respectively).

Actin Knockdown

The morpholino acta1ATG (5′-tctcgtcgtcgtcacacatcttgat-3′) was designed fully complementary to the translation start of *acta1b* and with two mismatches against *acta1a* and ordered from Gene Tools. Zebrafish embryos were injected at the 1-cell stage into the yolk with 1.4 nL of morpholino solution as described

previously (Berger et al., 2011). As controls, isogenic embryos from the same clutches were injected with injection solution (0.1% phenol red in water) and equivalent concentrations of standard control morpholino (5′-cctcttacctcagt tacaatttata-3′). The birefringence of morphants was normalized to larvae treated with injection solution.

Data and Accessibility

The grey values obtained by the birefringence assay have been deposited at Mendeley Data and are available at https://doi.org/10.17632/fd3f9nr2zr.1.

SUPPLEMENTAL INFORMATION

Supplemental Information includes Supplemental Experimental Procedures, seven figures, and one table and can be found with this article online at https://doi.org/10.1016/j.celrep.2017.12.069.

ACKNOWLEDGMENTS

We thank Monash Micro Imaging, the Monash Ramaciotti Centre for Cryo Electron Microscopy, and the Monash Biomedical Proteomics Facility for technical support. P.D.C., A.G.S., and J.B. were supported by the National Health and Medical Research Council of Australia (APP1084944, APP1024482, and APP1090408) and A.A. by the Swedish Research Council (2013-3003). The Australian Regenerative Medicine Institute is supported by grants from the state government of Victoria and the Australian government.

AUTHOR CONTRIBUTIONS

J.B. performed the experiments. S.B. performed histology. M.L. and A.A. conducted force measurements. A.S.J. initiated the simple sequence length polymorphism (SSLP) analysis. A.G.S. and N.B. modeled human CCT5. J.B. and P.D.C. conceived the experiments and wrote the manuscript, which was edited by all authors.

DECLARATION OF INTERESTS

The authors declare no competing interests.

Received: April 18, 2017
Revised: September 11, 2017
Accepted: December 19, 2017
Published: January 9, 2018

REFERENCES

Abramsson, A., Kettunen, P., Banote, R.K., Lott, E., Li, M., Arner, A., and Zetterberg, H. (2013). The zebrafish amyloid precursor protein-b is required for motor neuron guidance and synapse formation. Dev. Biol. *381*, 377–388.

Amsterdam, A., Nissen, R.M., Sun, Z., Swindell, E.C., Farrington, S., and Hopkins, N. (2004). Identification of 315 genes essential for early zebrafish development. Proc. Natl. Acad. Sci. USA *101*, 12792–12797.

Behrends, C., Langer, C.A., Boteva, R., Böttcher, U.M., Stemp, M.J., Schaffar, G., Rao, B.V., Giese, A., Kretzschmar, H., Siegers, K., and Hartl, F.U. (2006). Chaperonin TRiC promotes the assembly of polyQ expansion proteins into nontoxic oligomers. Mol. Cell *23*, 887–897.

Berger, J., and Currie, P.D. (2013). 503unc, a small and muscle-specific zebrafish promoter. Genesis *51*, 443–447.

Berger, J., Berger, S., Jacoby, A.S., Wilton, S.D., and Currie, P.D. (2011). Evaluation of exon-skipping strategies for Duchenne muscular dystrophy utilizing dystrophin-deficient zebrafish. J. Cell. Mol. Med. *15*, 2643–2651.

Berger, J., Sztal, T., and Currie, P.D. (2012). Quantification of birefringence readily measures the level of muscle damage in zebrafish. Biochem. Biophys. Res. Commun. *423*, 785–788.

Berger, J., Tarakci, H., Berger, S., Li, M., Hall, T.E., Arner, A., and Currie, P.D. (2014). Loss of Tropomodulin4 in the zebrafish mutant träge causes cytoplasmic rod formation and muscle weakness reminiscent of nemaline myopathy. Dis. Model. Mech. *7*, 1407–1415.

Bouhouche, A., Benomar, A., Bouslam, N., Chkili, T., and Yahyaoui, M. (2006). Mutation in the epsilon subunit of the cytosolic chaperonin-containing t-complex peptide-1 (Cct5) gene causes autosomal recessive mutilating sensory neuropathy with spastic paraplegia. J. Med. Genet. *43*, 441–443.

Dubey, J., Ratnakaran, N., and Koushika, S.P. (2015). Neurodegeneration and microtubule dynamics: death by a thousand cuts. Front. Cell. Neurosci. *9*, 343.

Erdmann, J., Stark, K., Esslinger, U.B., Rumpf, P.M., Koesling, D., de Wit, C., Kaiser, F.J., Braunholz, D., Medack, A., Fischer, M., et al.; CARDIoGRAM (2013). Dysfunctional nitric oxide signalling increases risk of myocardial infarction. Nature *504*, 432–436.

Etard, C., Armant, O., Roostalu, U., Gourain, V., Ferg, M., and Strähle, U. (2015). Loss of function of myosin chaperones triggers Hsf1-mediated transcriptional response in skeletal muscle cells. Genome Biol. *16*, 267.

Fontanella, B., Birolo, L., Infusini, G., Cirulli, C., Marzullo, L., Pucci, P., Turco, M.C., and Tosco, A. (2010). The co-chaperone BAG3 interacts with the cytosolic chaperonin CCT: new hints for actin folding. Int. J. Biochem. Cell Biol. *42*, 641–650.

Gao, Y., Thomas, J.O., Chow, R.L., Lee, G.H., and Cowan, N.J. (1992). A cytoplasmic chaperonin that catalyzes beta-actin folding. Cell *69*, 1043–1050.

Granato, M., van Eeden, F.J., Schach, U., Trowe, T., Brand, M., Furutani-Seiki, M., Haffter, P., Hammerschmidt, M., Heisenberg, C.P., Jiang, Y.J., et al. (1996). Genes controlling and mediating locomotion behavior of the zebrafish embryo and larva. Development *123*, 399–413.

Hein, M.Y., Hubner, N.C., Poser, I., Cox, J., Nagaraj, N., Toyoda, Y., Gak, I.A., Weisswange, I., Mansfeld, J., Buchholz, F., et al. (2015). A human interactome in three quantitative dimensions organized by stoichiometries and abundances. Cell *163*, 712–723.

Hishiya, A., Kitazawa, T., and Takayama, S. (2010). BAG3 and Hsc70 interact with actin capping protein CapZ to maintain myofibrillar integrity under mechanical stress. Circ. Res. *107*, 1220–1231.

Joachimiak, L.A., Walzthoeni, T., Liu, C.W., Aebersold, R., and Frydman, J. (2014). The structural basis of substrate recognition by the eukaryotic chaperonin TRiC/CCT. Cell *159*, 1042–1055.

Kapitein, L.C., and Hoogenraad, C.C. (2015). Building the Neuronal Microtubule Cytoskeleton. Neuron *87*, 492–506.

Li, M., Andersson-Lendahl, M., Sejersen, T., and Arner, A. (2013). Knockdown of desmin in zebrafish larvae affects interfilament spacing and mechanical properties of skeletal muscle. J. Gen. Physiol. *141*, 335–345.

Llorca, O., McCormack, E.A., Hynes, G., Grantham, J., Cordell, J., Carrascosa, J.L., Willison, K.R., Fernandez, J.J., and Valpuesta, J.M. (1999). Eukaryotic type II chaperonin CCT interacts with actin through specific subunits. Nature *402*, 693–696.

Lopez, T., Dalton, K., and Frydman, J. (2015). The Mechanism and Function of Group II Chaperonins. J. Mol. Biol. *427*, 2919–2930.

Lundin, V.F., Srayko, M., Hyman, A.A., and Leroux, M.R. (2008). Efficient chaperone-mediated tubulin biogenesis is essential for cell division and cell migration in C. elegans. Dev. Biol. *313*, 320–334.

Matsuda, N., and Mishina, M. (2004). Identification of chaperonin CCT gamma subunit as a determinant of retinotectal development by whole-genome subtraction cloning from zebrafish no tectal neuron mutant. Development *131*, 1913–1925.

Melkani, G.C., Bhide, S., Han, A., Vyas, J., Livelo, C., Bodmer, R., and Bernstein, S.I. (2017). TRiC/CCT chaperonins are essential for maintaining myofibril organization, cardiac physiological rhythm, and lifespan. FEBS Lett. *591*, 3447–3458.

Meyer, A.S., Gillespie, J.R., Walther, D., Millet, I.S., Doniach, S., and Frydman, J. (2003). Closing the folding chamber of the eukaryotic chaperonin requires the transition state of ATP hydrolysis. Cell *113*, 369–381.

Minegishi, Y., Sheng, X., Yoshitake, K., Sergeev, Y., Iejima, D., Shibagaki, Y., Monma, N., Ikeo, K., Furuno, M., Zhuang, W., et al. (2016). CCT2 Mutations

Evoke Leber Congenital Amaurosis due to Chaperone Complex Instability. Sci. Rep. *6*, 33742.

Muñoz, I.G., Yébenes, H., Zhou, M., Mesa, P., Serna, M., Park, A.Y., Bragado-Nilsson, E., Beloso, A., de Cárcer, G., Malumbres, M., et al. (2011). Crystal structure of the open conformation of the mammalian chaperonin CCT in complex with tubulin. Nat. Struct. Mol. Biol. *18*, 14–19.

North, K.N., Wang, C.H., Clarke, N., Jungbluth, H., Vainzof, M., Dowling, J.J., Amburgey, K., Quijano-Roy, S., Beggs, A.H., Sewry, C., et al.; International Standard of Care Committee for Congenital Myopathies (2014). Approach to the diagnosis of congenital myopathies. Neuromuscul. Disord. *24*, 97–116.

Pappas, C.T., Bhattacharya, N., Cooper, J.A., and Gregorio, C.C. (2008). Nebulin interacts with CapZ and regulates thin filament architecture within the Z-disc. Mol. Biol. Cell *19*, 1837–1847.

Pappenberger, G., McCormack, E.A., and Willison, K.R. (2006). Quantitative actin folding reactions using yeast CCT purified via an internal tag in the CCT3/gamma subunit. J. Mol. Biol. *360*, 484–496.

Pavel, M., Imarisio, S., Menzies, F.M., Jimenez-Sanchez, M., Siddiqi, F.H., Wu, X., Renna, M., O'Kane, C.J., Crowther, D.C., and Rubinsztein, D.C. (2016). CCT complex restricts neuropathogenic protein aggregation via autophagy. Nat. Commun. *7*, 13821.

Pereira, J.H., McAndrew, R.P., Sergeeva, O.A., Ralston, C.Y., King, J.A., and Adams, P.D. (2017). Structure of the human TRiC/CCT Subunit 5 associated with hereditary sensory neuropathy. Sci. Rep. *7*, 3673.

Petzold, A.M., Balciunas, D., Sivasubbu, S., Clark, K.J., Bedell, V.M., Westcot, S.E., Myers, S.R., Moulder, G.L., Thomas, M.J., and Ekker, S.C. (2009). Nicotine response genetics in the zebrafish. Proc. Natl. Acad. Sci. USA *106*, 18662–18667.

Radke, M.B., Taft, M.H., Stapel, B., Hilfiker-Kleiner, D., Preller, M., and Manstein, D.J. (2014). Small molecule-mediated refolding and activation of myosin motor function. eLife *3*, e01603.

Ravenscroft, G., Jackaman, C., Sewry, C.A., McNamara, E., Squire, S.E., Potter, A.C., Papadimitriou, J., Griffiths, L.M., Bakker, A.J., Davies, K.E., et al. (2011). Actin nemaline myopathy mouse reproduces disease, suggests other actin disease phenotypes and provides cautionary note on muscle transgene expression. PLoS ONE *6*, e28699.

Reissmann, S., Joachimiak, L.A., Chen, B., Meyer, A.S., Nguyen, A., and Frydman, J. (2012). A gradient of ATP affinities generates an asymmetric power stroke driving the chaperonin TRIC/CCT folding cycle. Cell Rep. *2*, 866–877.

Sanger, J.W., Wang, J., Fan, Y., White, J., and Sanger, J.M. (2010). Assembly and dynamics of myofibrils. J. Biomed. Biotechnol. *2010*, 858606.

Sergeeva, O.A., Chen, B., Haase-Pettingell, C., Ludtke, S.J., Chiu, W., and King, J.A. (2013). Human CCT4 and CCT5 chaperonin subunits expressed in Escherichia coli form biologically active homo-oligomers. J. Biol. Chem. *288*, 17734–17744.

Sot, B., Rubio-Muñoz, A., Leal-Quintero, A., Martínez-Sabando, J., Marcilla, M., Roodveldt, C., and Valpuesta, J.M. (2017). The chaperonin CCT inhibits assembly of α-synuclein amyloid fibrils by a specific, conformation-dependent interaction. Sci. Rep. *7*, 40859.

Srikakulam, R., and Winkelmann, D.A. (1999). Myosin II folding is mediated by a molecular chaperonin. J. Biol. Chem. *274*, 27265–27273.

Stoldt, V., Rademacher, F., Kehren, V., Ernst, J.F., Pearce, D.A., and Sherman, F. (1996). Review: the Cct eukaryotic chaperonin subunits of Saccharomyces cerevisiae and other yeasts. Yeast *12*, 523–529.

Sztal, T.E., Zhao, M., Williams, C., Oorschot, V., Parslow, A.C., Giousoh, A., Yuen, M., Hall, T.E., Costin, A., Ramm, G., et al. (2015). Zebrafish models for nemaline myopathy reveal a spectrum of nemaline bodies contributing to reduced muscle function. Acta Neuropathol. *130*, 389–406.

Tam, S., Geller, R., Spiess, C., and Frydman, J. (2006). The chaperonin TRiC controls polyglutamine aggregation and toxicity through subunit-specific interactions. Nat. Cell Biol. *8*, 1155–1162.

Vainberg, I.E., Lewis, S.A., Rommelaere, H., Ampe, C., Vandekerckhove, J., Klein, H.L., and Cowan, N.J. (1998). Prefoldin, a chaperone that delivers unfolded proteins to cytosolic chaperonin. Cell *93*, 863–873.

Yaffe, M.B., Farr, G.W., Miklos, D., Horwich, A.L., Sternlicht, M.L., and Sternlicht, H. (1992). TCP1 complex is a molecular chaperone in tubulin biogenesis. Nature *358*, 245–248.

Yam, A.Y., Xia, Y., Lin, H.T., Burlingame, A., Gerstein, M., and Frydman, J. (2008). Defining the TRiC/CCT interactome links chaperonin function to stabilization of newly made proteins with complex topologies. Nat. Struct. Mol. Biol. *15*, 1255–1262.